

Experimental evidence of T_c enhancement above
50 K and diode and paramagnetic-Meissner effects,
in Nickelate films on highly reduced $SrTiO_3$

Anna Eyal^{1†} and Gad Koren^{1*†}

^{1*}Physics Department, Technion, Haifa, 32000, Israel.

*Corresponding author(s). E-mail(s): gkoren@physics.technion.ac.il;

Contributing authors: anna.eyal@gmail.com;

[†]These authors contributed equally to this work.

Keywords: Nickelates, Superconductivity, Diode effect, Paramagnetic Meissner effect

Since the discovery of superconductivity in nickelate thin films in 2019, the quest for enhancing their T_c has been ongoing. Here we provide experimental evidence for T_c enhancement in oxygen deficient films on highly reduced and conducting $SrTiO_3$ substrates. T_c onset of 50-70 K was found in Meissner and transport measurements, which indicates superconductivity in islands or domains in our films, where T_c of zero resistance is obtained at 20-25 K. In addition, we observed a giant paramagnetic-Meissner effect peak at about 48 K, which further supports the existence of a superconductive transition just above it. Furthermore, an asymmetric or nonreciprocal and non-hysteretic superconductive diode effect was observed. The later could be fully polarized, and its polarity could be reversed. The specific phase responsible for these

notable effects was not yet identified, and further research is needed in order to identify and isolate the relevant phase.

1 Introduction

The discovery of superconductivity in nickelate thin films by the Hwang group in 2019 [Li et al \(2019\)](#) ignited worldwide interest in this new family of materials [Norman \(2020\)](#); [Li et al \(2020a\)](#); [Osada et al \(2020\)](#); [Li et al \(2020b\)](#); [Zhou et al \(2020, 2024\)](#); [Zeng et al \(2020\)](#); [Gu et al \(2020\)](#); [Lee et al \(2023\)](#). Given their similarity to cuprates, nickelates were immediately recognized as a potential new platform for high-temperature superconductivity, as discussed in an early review by [Norman \(2020\)](#). Initial studies focused on mapping the phase diagram of these $\text{Nd}_{0.8}\text{Sr}_{0.2}\text{NiO}_2$ (112 phase) films and characterizing their fundamental properties [Li et al \(2020a\)](#). Soon after, superconductivity was also observed in $\text{Pr}_{0.8}\text{Sr}_{0.2}\text{NiO}_2$ thin films [Osada et al \(2020\)](#), reinforcing the idea that superconductivity could emerge in multiple members of the nickelate family. However, in both this study and in Ref. [Li et al \(2019\)](#) the films thickness ranged between 5 and 12 nm only. Thicker films of this kind showed no superconductivity in bulk form [Li et al \(2020b\)](#); [Zhou et al \(2020\)](#), and raised the question whether the observed superconductivity in thin films of a few nanometers is an interface effect originating in strains or other interactions with the substrate. More recently, fabrication of free-standing superconducting nickelate films was demonstrated, and a maximum T_c of 25 K was found in films on (110) NdGaO_3 [Lee et al \(2024\)](#). Even higher superconducting T_c values above 30 K at ambient pressure were obtained in ultra thin films of $\text{Sm}_{1-x-y-z}\text{Eu}_x\text{Ca}_y\text{Sr}_z\text{NiO}_2$ also on NdGaO_3 wafers [Chow et al \(2024\)](#). The highest T_c so far, of approximately 80 K, was found in well oxygenated single crystals of the double-layer nickelate $\text{La}_3\text{Ni}_2\text{O}_7$ (327 phase) under high pressure of tens of GPa [Sun et al \(2023\)](#). Another study demonstrated bulk superconductivity in the nickelates, where the reduction process in CaH_2

of perovskite $La_{1-x}Ca_xNiO_3$ single crystals yielded the superconducting infinite layer $La_{1-x}Ca_xNiO_{2+\delta}$ phase [Puphal et al \(2021\)](#). However, this also led to cracking of these superconducting crystals. Very recently, three studies were reported in which an ambient pressure superconducting T_c onset over 40 K was found in the bilayer 327 phase of nickelate films [Ko et al \(2024\)](#); [Zhou et al \(2024\)](#); [Liu et al \(2025\)](#). In these works, an oxidation annealing step in Ozone was employed in order to get the high T_c phase, unlike previous works on nickelate films where a reduction annealing process, generally in CaH_2 , was used. The highest T_c onset in these studies was obtained in strained $La_2PrNi_2O_7$ films with T_c onset of 48 K by Liu et al. [Liu et al \(2025\)](#).

In earlier studies, most films showing signs of superconductivity were prepared in a two-step process, whereby the perovskite films were deposited first, followed by a second step of reduction in CaH_2 . These films, usually with thicknesses of a few to several nm, were comprised of the infinite layer 112 phase, possibly in close proximity to the substrate, as the carrier of the superconductive currents. In the most recent study of films of the 327 bilayer phase [Liu et al \(2025\)](#), laser deposition was still used but at a much lower fluence on the target and this was followed by Ozone oxidation. In the present study, we followed the earlier two-steps route and prepared the perovskite phase first, like other groups did. But unlike other groups, the reduction in CaH_2 step was carried out under pumping (see methods for details). This led to an effective reduction not only of the films but also of the $SrTiO_3$ (STO) substrate, which became black and highly conductive. After this annealing process, AFM images of the films showed good crystallinity, and magnetic moment measurements versus temperature showed a T_c onset at about 50 K. Furthermore, resistance versus temperature of our films showed a T_c onset of 60-70 K and T_c offset with zero resistance at 20-25 K. Therefore, the higher T_c indicates superconductivity in islands, where the lower transition to zero resistance superconductivity is due to the weak-links between

them becoming superconducting as well.

In this study we also observed two additional effects. One is a highly asymmetric diode effect in the voltage versus current curves (VICs) without an external magnetic field, where under one polarity of the bias current an Ohmic behavior was found, while in the opposite polarity a supercurrent was observed. However, the sign of this effect could be reversed depending on the distance between the contacts used. This kind of diode effect was recently observed by Qi et al. in BSCCO Qi et al (2025), and theoretically investigated by Mori et al. where a sign reversal was found Mori et al (2025). The other observation is of a giant paramagnetic Meissner effect peak (PME, also known as the Wohlleben effect Braunisch et al (1993)), where a positive magnetization peak appears just below the superconducting transition at about 50 K. This might indicate odd-frequency superconductivity Linder and Balatsky (2019), the presence of SN or SF junctions in our samples Koblichka et al (2023) or the development of a giant vortex state Moshchalkov et al (1997). The PME peaks were most prominent under magnetic fields of thousands Oersted normal to the wafer, unlike earlier studies where fields around one Oersted were used Braunisch et al (1993).

We believe that the main reason for our extraordinary results originates in the combination of highly reduced black STO substrates and the nickelate films. Stand-alone wafers of pure black STO were metallic, highly conductive and had a superconducting transition at T_c of 0.25 K, similarly to optimally doped reduced STO Lin et al (2014). In some cases, we identified the superconductive phase by XRD as due to the infinite-layer $\text{Nd}_{0.8}\text{Sr}_{0.2}\text{NiO}_2$ as other groups have found, but in other cases, XRD of our reduced films showed no particular features beyond the disappearance of the perovskite phase. This could be due to the relatively low resolution and high noise level in our XRD system. In both type of cases though, signature of T_c

above 50 K was observed. TEM experiments to identify the phases in our films are underway at the present time, but we have no results yet. There is still the possibility that we have mixed nickelate phases in our films as found by Zhang et al. [Zhang et al \(2025\)](#), where single layers, bilayers and trilayers of the parent $(NdSr)_3Ni_2O_7$ phase were observed in the same sample by TEM images. Nevertheless, we do have some supporting AFM indications that polymorphs of the 327 phase such as the 2222 or 1313 are present in our films [Chen et al \(2024\)](#).

2 Experimental

All our Nickelate films were prepared by pulsed laser deposition (PLD) on optically polished Ti-terminated (100) STO wafers of $10 \times 10 \text{ mm}^2$ area, using a ceramic target of $Nd_{0.8}Sr_{0.2}NiO_3$ (NSNO). Figure 1 shows the surface morphology of a BHF etched and $1000^\circ\text{C}/4\text{h}$ annealed STO substrate with one unit cell steps (a), together with the surface morphology of a 30 nm thick NSNO1red1h film grown on it (reduced for 1 h in CaH_2 at 320°C) (b). There were many holes in this film of about 2 nm depth as shown by the line profile in (c). This could be attributed to the presence of $(NdSr)_3Ni_2O_7$ polymorphs of the 2222 or 1313 type in our films, that have *c*-axis unit cell of ~ 2 nm [Chen et al \(2024\)](#). In our previous work on NSNO in 2021 [Koren et al \(2021\)](#) we used the third harmonic of a Nd-YAG laser with 355 nm wavelength to deposit the films. This did not yield a dominant perovskite phase of the Nickelate films, as the (001) peak of these films was absent or too weak to be seen. We stress that this was not due to limited resolution of our XRD measurements, since in similar manganite films of $Nd_{2/3}Sr_{1/3}MnO_3$, all (00*n*) peaks were clearly resolved, including the odd-*n* ones.

In the present study, we used the fourth-harmonic of the Nd-YAG laser with 266 nm wavelength and this yielded the desired perovskite phase with all the (00*n*) peaks

as depicted in Fig. 1 (d)-(f). Apparently, the deeper UV wavelength is necessary for obtaining the perovskite phase in the Nickelates. This is in contrast to $YBa_2Cu_3O_{7-\delta}$ (YBCO) where all the Nd-YAG harmonics yielded a stable perovskite phase [Koren et al \(1989\)](#). Films of 10, 20, 30 and 35 nm thickness were prepared, at 780⁰C heater block temperature (\sim 600⁰C wafer temperature) and 100 mTorr O₂ flow. The 266 nm laser operated at 3.3 Hz and focused to 1.5-2 J/cm² on the target. This was followed by adding 10 Torr of oxygen and cooling down to room temperature with a dwell of 1 hour at 450⁰C. We generally cut our STO wafers with the virgin NSNO films into four quarters of 5×5 mm² area, for processing and measurements under different annealing conditions.

Reduction or annealing of the films was carried out in aluminum packets with 0.35 g of CaH_2 powder at about 320⁰C, for various durations between one and six hours. Highly resistive films were obtained when using closed packets. However, when a small aperture in the packets was made and the annealing was performed under pumping in a chamber with a base pressure of 10⁻⁷ Torr at 25⁰C, low resistance films had been produced. During the actual reduction process at 320⁰C, the pressure in the vacuum chamber rose to about 5-10×10⁻⁷ Torr, while inside the packet we estimate that a pressure of around 10⁻⁵ Torr was obtained due to the differential pumping used. Unlike in other studies, under our annealing conditions also the STO wafers were reduced and became black, metallic and highly conductive (apparently on the surface). This was also tested on bare STO wafers without the NSNO films, and the resulting black wafers were also superconducting at 0.25 K as found in the literature for optimally reduced STO [Lin et al \(2014\)](#).

3 Results

3.1 Short reduction time film

We start by presenting magnetic rather than resistive transport properties of our films. Figure 2 (a) shows XRD results of a virgin 30 nm thick NSNO1 film together with this film after reduction in CaH_2 at 320°C for 1 h to produce NSNO1red1h. One can see that the perovskite (002) peak of the virgin film disappeared in the reduced film, while a broad (002) peak of the infinite-layer $Nd_{0.8}Sr_{0.2}NiO_2$ phase appeared. We stress that no other clear film's peaks were observed in the $10^\circ < 2\theta < 140^\circ$ range of this XRD spectrum (see Fig. 1 of section S1 in the Supplemental for a similar film). Such peaks could be below the noise level of our x-ray system or hidden by the giant (n00) peaks of the STO substrate. The magnetic moment as a function of temperature of the reduced film is shown in Fig. 2 (b), where a zero field cooling (ZFC) to 1.8 K was performed, followed by applying a magnetic field of 20 Oe and measuring the moment while heating the sample, as in standard Meissner effect measurement.

Two superconducting transitions are seen in Fig. 2 (b). A sharp one of the infinite-layer phase with T_c onset at about 7 K, and a more moderate one with T_c onset at about 50 K of a possible different phase. Figure 2 (c) depicts the moments versus temperature at a few low fields, showing that their magnitude is proportional to the fields used, and also that the transition onset temperature is slightly suppressed with increasing field. We point out that the moments in Fig. 2 (b) are negative while in Fig. 2 (c) they are positive. This seemingly puzzling result is due to the magnetic history of the film and substrate preceding the measurements of the moments. The hysteretic moments versus field of Fig. 2 (d) clearly explains this behavior, as a previous history of high negative fields (-5000 Oe here) will yield negative moments at low fields and vice versa. The hysteresis in this figure also suggests the existence of ferromagnetism in the STO substrate with a coercive field of about 800 Oe. This was

established by measuring a bare STO wafer (without a film), where results similar to Fig. 2 (d) were found (see Fig. 2 in section S2 of the supplemental).

We now turn to the transport results of this film before and after annealing for 1 h in CaH_2 . Figure 3 shows the corresponding resistance versus temperature of these films, together with a typical background result of a bare black STO wafer also annealed in CaH_2 but for 6 h. The normal resistance at 100 K is $\sim 1 \Omega$ in the reduced film and that of the black STO is about an order of magnitude lower. However, we can't calculate the resistivity of our films since both film and substrate are conducting, we don't know how thick the conducting layer in the STO is, and we actually have a bilayer with interactions between the layers. Therefore, comparison with ρ values obtained in previous studies can't be made. A transition T_c of about 70 K is clearly seen in the CaH_2 annealed film, with crossing of the black STO curve at ~ 35 K and a drop of more than two orders of magnitude in the resistance down to the noise level below $1 \text{ m}\Omega$ at about 25 K. This indicates conduction between superconductive islands below 70 K via inter-islands weak-links, which become superconductive at T_c offset of 25 K. We believe this is the highest T_c onset reported at ambient pressure in reduced Nickelate films and it might originate in the bilayer 327 phase as observed in the high pressure experiments [Sun et al \(2023\)](#) (though in these experiments the Nickelate single crystals were well oxygenated and not reduced). However, we do not yet have conclusive TEM images of our films to prove this hypothesis. Figure 3 also shows that besides the fact that the normal black STO resistance is about an order of magnitude lower than that of the Nickelate film, this STO has a superconducting transition T_c at 0.25 K as depicted in the inset to this figure. This is typical of oxygen deficient, optimally reduced STO as reported in the literature [Lin et al \(2014\)](#).

3.2 Longer reduction time film

The strikingly high T_c values observed in our reduced film at ambient pressure, compelled us to double check these results and repeat the experiments on a second freshly prepared film. Figure 4 (a) shows an AFM image of a 30 s BHF etched and $1000^{\circ}\text{C}/4\text{h}$ annealed STO wafer on which this new NSNO2 film was deposited. The line-profile in (d) along the line shown in (a), shows that the terraces in (a) are of one unit cell height of the STO wafer (~ 0.4 nm). The laser fluence on the target was a bit higher than in the original NSNO1 film (2 versus 1.5 J/cm^2), resulting in a film thickness of 35 nm. Figure 4 (b) depicts an AFM image, and Fig. 4 (c) a typical line-profile along the line shown in (b), of the resulting virgin film. One can see many particulates and out-growths of 10-25 nm height on this film, and good crystallization at the background with grain sizes of about 50 nm. Unlike in Fig. 1 (b) of the NSNO1red1h film, we didn't observe the 2 nm deep holes in the freshly prepared and annealed one. This is probably due to the longer reduction time of 6 h in CaH_2 as compared to the 1 h used before, but under the same temperature (320°C). An AFM image of the resulting reduced NSNO2red6h sample is shown in Fig. 4 (e), while a line-profile along the line shown in it is given in (f). The reduced film shows a remarkable crystallization, where the particulate in (b) decreased in height to about 10 nm, developed a clear rectangular shapes along the (110) terraces of the STO wafer, and had background grain sizes of ~ 100 nm.

Magnetization measurements versus temperature of the oxygen deficient sample are shown in Fig. 5 (a), (b) and (c). In this set of measurements, the standard Meissner procedure of zero field cooling, followed by applying the field at 1.8 K and measuring the moments while heating, was followed by an oscillative field zeroing at 300 K, to ensure that the field was actually close to zero (and for the initial

cooldown, even less than 0.02 Oe) in the next ZFC. As can be seen in (a), a Meissner effect is apparent, above a small magnetic background from the STO substrate. The transition again isn't sharp, yet it is clear that the transition temperature is at about 50 K. In Fig. 5 (b) moment results are shown for two higher fields with their corresponding black STO background. Also shown are the net film signals after subtraction of their STO backgrounds. We note that this time, both film and bare STO wafer went through the same 6 h annealing in CaH_2 . The new feature observed under these fields is an emerging positive peak just below 50 K. This peak can be attributed to the paramagnetic Meissner effect (PME), which generally appears just below the superconducting transition temperature [Braunisch et al \(1993\)](#).

The appearance of the PME can be explained theoretically as due to the presence of an odd-frequency order parameter, the existence of SN or SF junctions in our films, or a giant vortex state in them [Linder and Balatsky \(2019\)](#); [Koblischka et al \(2023\)](#); [Moshchalkov et al \(1997\)](#). Junctions are quite obviously present in our films, as depicted in the schematic diagram of the inset to Fig. 6. This will be elaborated on in more details in the discussion section. More systematic measurements were carried out under fields of 2000 to 4000 Oe as shown in Fig. 5 (c), where the giant PME peaks are clearly larger than the magnitude of the whole Meissner effect drop with decreasing temperature. We note that the magnitude of these Meissner drops decrease with increasing field, and disappear at 4000 Oe, though the moment at temperatures above the PME peaks are always higher than just below it (see the dashed lines). The main point though of the observation of a giant PME at ~ 48 K in our films, is to further support the existence of superconductivity with T_c slightly above it at 50 K. In Fig. 5 (d) we plot on a lg-lg scale the net PME peak magnitude versus field and find a power law behavior with an exponent of $3/2$. We know of no theory to explain this behavior at the present time.

Transport results of R versus T of NSNO2red6h are shown in Fig. 6 together with the black STO background (times 10). T_c onset here is again at 70 K as in Fig. 3 on NSNO1red1h, but the transition to superconductivity doesn't go to zero and ends with a finite resistance at 1.8 K. This however, is an artifact produced by the PPMS measuring system, since in the low temperatures regime below ~ 20 K the voltage versus current curves at low bias are very asymmetric as can be seen in Fig. 7. Actually, they show a clear diode effect which will be discussed later on. Here we shall only point out that the PPMS system calculates the low bias resistance from both the resistive and superconductive parts of these curves, thus yielding a misleading finite resistance result. If one takes only the flat superconductive part of the V vs I curves of Fig. 7, one gets supercurrents and the resistance drops to its noise level. R calculated from such VICs are plotted by the red dots in Fig. 6. This shows a near-coincidence with the PPMS results above 25 K, with a sharp drop below it. Comparing the results of Fig. 6 and Fig. 3, one sees that the R drop in Fig. 3 is more moderate but it starts already at 50 K. Nevertheless, in both cases the R values drop to the noise level at about ~ 20 K and ~ 25 K, respectively. We thus conclude that the basic Meissner and T_c properties of both NSNO1red1h and NSNO2red6h films are quite similar. The differences in the observation of the giant PME peak and asymmetric diode effect in NSNO2red6h might be attributed to the longer annealing duration of this film. In the supplemental in sections S3 and S4, we present data of two more films we measured, of 10 and 20 nm thickness, with varying annealing times, that support the $T_c > 50$ K enhancement result here.

Next we present the diode effect and supercurrent results of NSNO2red6h as shown in Figs. 7 and 8. We start with Fig. 7 (a) and (b) where the ramping up of the current is separated from the ramping down by their respective colors (black and green). One can see that the V vs I curves here have two typical kinds of noise. The

standard voltage noise with peak to peak amplitude of about $5 \mu\text{V}$, and a telegraph noise jumps of about $7 \mu\text{V}$. These noises are almost averaged out to about $12 \mu\text{V}$ when sampling on a larger number of points (2000 vs 1000 points in (b) and (a), respectively). A remarkable feature in Fig. 7 is the observation of highly asymmetric curves which indicates a clear diode effect. We extract the supercurrents from the flat horizontal parts of these curves as depicted by the blue lines in Fig. 7. For instance, at 12 K in (c) one can see a small flat part with still asymmetric resistances on both its sides. This resistance asymmetry is almost gone at 20 K as seen in (d). We note that the whole V vs I curves here are shifted to small positive voltages. The shift is 0.35 mV at 1.8 K, while with increasing temperature it decreases to 0.22 mV at 20 K. This voltage shift behavior vs temperature can be better seen in the current vs voltage curves in Fig. 8 (c), where at 50 K it completely disappears. These voltage shifts are unclear to us at the present time, but they could arise from thermo-electric effects between the voltage contacts.

Figure 8 presents the more standard current versus voltage curves (IVCs) and the supercurrents versus temperature. The main differences between Fig. 7 and Fig. 8 are that the former represents raw data measured with one week old Ag-paste contacts, while the later shows smoothed data measured on freshly prepared Ag-paste contacts. Fig. 8 (a) and (b) shows how the $\pm 2.5 \mu\text{V}$ criterion to determine the critical current was used (see the shaded rectangles). It also shows that while in (b) the diode effect is fully asymmetric (resistance starts immediately above zero bias), in (a) the asymmetry shows both positive and negative supercurrents (I_c^+ and I_c^- , respectively). In Fig. 8 (c), a few IVCs are plotted, and the resulting combined supercurrents $I_c^+ + |I_c^-|$ as extracted from these and more IVCs are given versus temperature in (d). We note that below about 5 K, $I_c^+ + |I_c^-|$ in Fig. 8 (d) should actually be higher than 1 mA as can be deduced from Fig. 7 (a) which was obtained with different contacts and

without averaging.

4 Discussion

In the present study, experimental evidence for three novel phenomena in nickelate films was found. T_c enhancement to 50-70 K at ambient pressure, a giant paramagnetic Meissner effect peak around 48 K, and a polarity-reversible diode effect. To the best of our knowledge, T_c above 50 K as found here is the highest reported in reduced nickelate films. Since this effect seems to be strongly dependent on the highly reduced STO substrate, we decided to repeat the experiment on a different new film but with a longer annealing time. The high T_c observed was well reproduced in this new film, but in addition giant PME peak and diode effects were discovered. In the following, we discuss these three phenomena.

4.1 T_c enhancement

Ever since the discovery of superconductivity in reduced nickelate thin films [Li et al \(2019\)](#), the quest to increase their T_c has been ongoing. By better controlling the deposition, composition and annealing in CaH_2 conditions, success was achieved but it seems the substrate on which the films were deposited, played a major role in obtaining the highest T_c value. Instead of the commonly used STO substrate, the use of $NdGaO_3$ substrates yielded the highest T_c values so far (25 and 38 K) [Lee et al \(2024\)](#); [Chow et al \(2024\)](#). In our study, we still use the STO substrate, but in a highly reduced and conducting state and this seems to be the essential ingredient in pushing T_c up. The lattice constant of reduced and normal STO are almost the same [Yamada and Miller \(1973\)](#), therefore the increased T_c doesn't originate in strains in our case. This conclusion is also strengthened by the fact that the present films in which T_c was enhanced are 30-35 nm thick, too thick to be affected by strain with the substrate,

unless this is an interface effect. The later is actually the case, as can be deduced from Figs. 3 and 4 of the supplemental results obtained in 20 and 10 nm thick films.

If in fact, the film's layers in close proximity with the substrate are responsible for the elevated T_c observed, then the top layers of the film serve to protect the bottom layers from ambient effects, and the reduced substrate serves as an effective oxygen getter, keeping the film well reduced over time. We noticed aging effects of our films in which over a few months became very resistive, and the STO substrates lost their blackness and returned to their normal whitish transparent color. This obviously originated in the reduced STO absorbing oxygen from the air, indicating its strong efficiency as a getter even at room temperature.

Next we try to identify the phase or phases involved in the elevated T_c in the present study. Figure 2 (b) clearly shows that we have two Meissner transition temperatures in NSNO1red1h which was reduced in CaH_2 for 1 h. The XRD in Fig. 2 (a) points to the presence of the infinite-layer nickelate phase, that was reported already in the pioneering study in which superconductivity in the nickelates was first observed [Li et al \(2019\)](#). It is possible that this phase with a strong gettering effect by the black STO substrate is also responsible for the elevated transition at 50 K. However, a reason against this scenario can be found in Fig. 5 (a) where the low T_c transition at 7 K is absent, but the 50 K one is still robust. Also, the XRD of this NSNO2red6h film shows no film peaks besides the huge STO peaks (see Fig. 1 of section S1 in the supplemental), even though Fig. 4 (e) reveals good crystallization of this film. We note that this result can be due to high noise level in our x-ray machine, or to peaks coincidence with those of the STO wafer. In addition, as mentioned before, a scenario of mixed phases in our films is still possible, and this might smear the XRD results. Such a mixture of single layer $(NdSr)_2NiO_4$, bilayer $(NdSr)_3Ni_2O_7$, and trilayer

$(NdSr)_4Ni_3O_{10}$ phases was found in the parent 327 phase after various annealings in oxygen [Zhang et al \(2025\)](#). So, the question of what phase or phases are responsible for the present elevated T_c remains and awaits ongoing TEM measurement results that could identify them.

4.2 Meissner and PME effects

Observation of the Meissner effect is a clear signature of superconductivity. It can be seen here in Fig. 2 (b) and Fig. 5 (a) where zero field cooling was followed by heating under 20 Oe. The former shows the low temperature superconducting transition of the $Nd_{0.8}Sr_{0.2}NiO_2$ infinite-layer phase with $T_c \sim 7$ K, together with the $T_c \sim 50$ K phase or phases. This was obtained in a film that was reduced in CaH_2 for 1 h only. When the reduction time was increased to 6 h on a different film as in Fig. 5, the low-temperature phase disappeared and only the high-temperature one persisted. Further support for the notion that the $T_c \sim 50$ K transition originates in superconductivity, is given in Fig. 5 (c) where a giant paramagnetic Meissner effect peak appears at ~ 48 K. Such a peak signifies the presence of superconductivity with a transition temperature slightly above it.

The PME peak can be attributed to odd-frequency order parameter which breaks inversion and time reversal symmetries [Linder and Balatsky \(2019\)](#). It could also originate in SN or SF junctions in our film [Koblischka et al \(2023\)](#), or develop from the formation of a giant vortex state in them [Moshchalkov et al \(1997\)](#). We can not comment on the order parameter symmetry in our films, since we do not have scanning tunneling conductance spectroscopy results on them. It would be interesting to have such data, to prove or refute the odd-frequency nature of the order parameter. The presence of NS or NF junctions in our films is easier to envision from the inset to Fig.

6, where such junctions form at the interface of the superconducting islands and the STO wafer, or between the islands themselves. The vortex state scenario in our films is quite possible, in particular since the robust PME peaks are observed at quite high fields (2000-4000 Oe). Non-equilibrium vortex trapping due to pinning sites or surface barriers could result in delayed vortex relaxations showing a paramagnetic response. Such a PME peak, but of a much smaller magnitude, was observed in cuprates under fields of a few Oe [Riedling et al \(1994\)](#).

4.3 Diode effect

Another interesting phenomenon observed in our films is the diode effect as presented in Figs. 7 and 8. The best way to observe this effect is via the voltage versus current curves (VICs) as depicted in Fig. 7 for a few temperatures. In general, a superconducting diode effect (SDE) can be observed in hysteretic (or nonreciprocal) superconductive Josephson junctions, where the supercurrents with increasing and decreasing bias currents are different $I_c^+ \neq |I_c^-|$. Then, when using a modulated bias current with amplitude in between these two supercurrents, the system will alternate between resistive and non-resistive states, which is the basic rectifying diode effect [Qi et al \(2025\)](#). Here, in Fig. 7 (a) to (c) one can see *fully polarized* VICs, where on negative bias the films are resistive, while on positive bias they are superconducting. In (d), very close to T_c of zero resistance, the VIC is almost Ohmic all the way with only a tiny supercurrent part. We emphasize that there is almost no hysteresis in our case, and our SDE is more like the diode effect seen in semi-conductors but with a zero resistance in the more conductive branch. Theoretically, the SDE originates in materials with broken time-reversal and inversion symmetries [He et al \(2022\)](#); [Ilić and Bergeret \(2022\)](#); [Yuan and Fu \(2022\)](#); [Ando et al \(2022\)](#). Most of these studies assumed the presence of an external magnetic field, but some discussed also field-free SDE [Qi et al \(2025\)](#). Internal Zeeman fields and disorder in nonreciprocal materials

with strong spin-orbit or Rashba interactions, can also facilitate field-free SDE [Ilić and Bergeret \(2022\)](#).

To our surprise, the observed SDE was easily polarity reversed as can be seen in Fig. 8 (a) to (c). This was found on the *same* film as in Fig. 7, but with newly prepared contacts with obviously a slightly different geometry. Mori et al. showed theoretically that by changing the distance between the superconducting electrodes, the SDE polarity could be reversed and that this effect is periodical in distance [Mori et al \(2025\)](#). So in our case, the superconducting islands or domains can be considered as S-electrodes, and the black STO as the connecting normal metal (N-electrode) in the Mori et al. scenario. It should be noted that as long as there is no percolative supercurrent in the nickelate film (between T_c onset and $T_c(R=0)$), the bias current will mostly flow via the highly conductive normal STO wafer, with occasional shunts through adjacent superconducting islands, as depicted in the schematic drawing of the inset to Fig. 6.

4.4 Supercurrents

Figures 7 and 8 were used to determine the supercurrents versus temperature in our film, as depicted in Fig. 8 (d). Due to the asymmetric VICs with different I_c^+ and $|I_c^-|$, we determined the combined supercurrents as $I_c^+ + |I_c^-|$. In the symmetric VIC case, it would amount to $2I_c$, while in the fully Asymmetric case (as in Fig. 7), it would be the standard I_c . We used a $\pm 2.5 \mu V$ criterion to assess the combined supercurrent. This criterion can be inferred from the noise of the VICs of Fig. 7 (a) and (b) at 1.8 K. The uninterrupted trace voltage noise is about $5 \mu V$ ($2\sigma_1$), while the occasional telegraph-jumps are about $7 \mu V$. Thus, the overall noise is about $12 \mu V$ ($2\sigma_2$). Disregarding the telegraph-noise which is less prevalent at higher temperatures, we end

up with the $\sigma_1 = 2.5 \mu\text{V}$ criterion. Fig. 8 (d) shows that the supercurrent in our film dies off at about 25-30 K, and is zero at 50 K. Therefore, much optimization work is needed to push the supercurrent to a higher temperature, closer to T_c onset at 50-70 K. Needless to say that identifying the phase and poly-morphs responsible for this high T_c onset would help attain this goal. Finally, we stress again that the present high T_c results are different from those obtained in the well oxygenate $\text{La}_3\text{Ni}_2\text{O}_7$ phase [Sun et al \(2023\)](#); [Ko et al \(2024\)](#); [Zhou et al \(2024\)](#); [Liu et al \(2025\)](#), in that our nickelate films are highly oxygen deficient and strongly affected by the highly reduced black STO substrate.

5 Conclusions

In this study, we demonstrated three noteworthy phenomena in oxygen-deficient nickelate thin films on highly reduced black STO substrates: A T_c onset enhancement to 50-70 K, a giant paramagnetic Meissner effect peak, and a highly asymmetric nonreciprocal superconductive diode effect. All of these results were obtained on highly reduced and highly conducting black STO substrates, which are essential for the present observations. The exact phase responsible for these effects is not yet identified, but it is most likely to be the 327 bilayer nickelate phase and its poly-morphs. Further research is needed to identify the phase or phases that are at the origin of these remarkable phenomena in nickelate films.

6 Figures

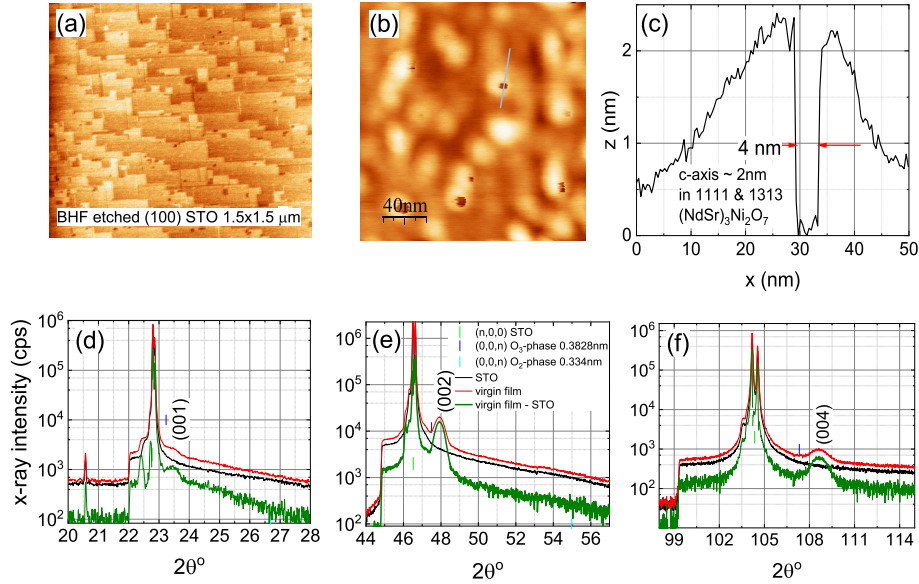


Fig. 1 AFM images of STO and NSNO1red1h, and XRD spectra of the 30 nm thick NSNO1 virgin film. (a) shows the surface morphology of the BHF etched and annealed STO wafer with its typical terraces, on which the NSNO1 film was deposited. (b) depicts the surface morphology of the reduced film NSNO1red1h, where a few holes can be seen whose typical line-profile along the line marked in (b) is given in (c). (d)-(f) show XRD results of NSNO1, where all (00n) film peaks of the $Nd_{0.8}Sr_{0.2}NiO_3$ perovskite phase are seen, except for the weakest (003) peak.

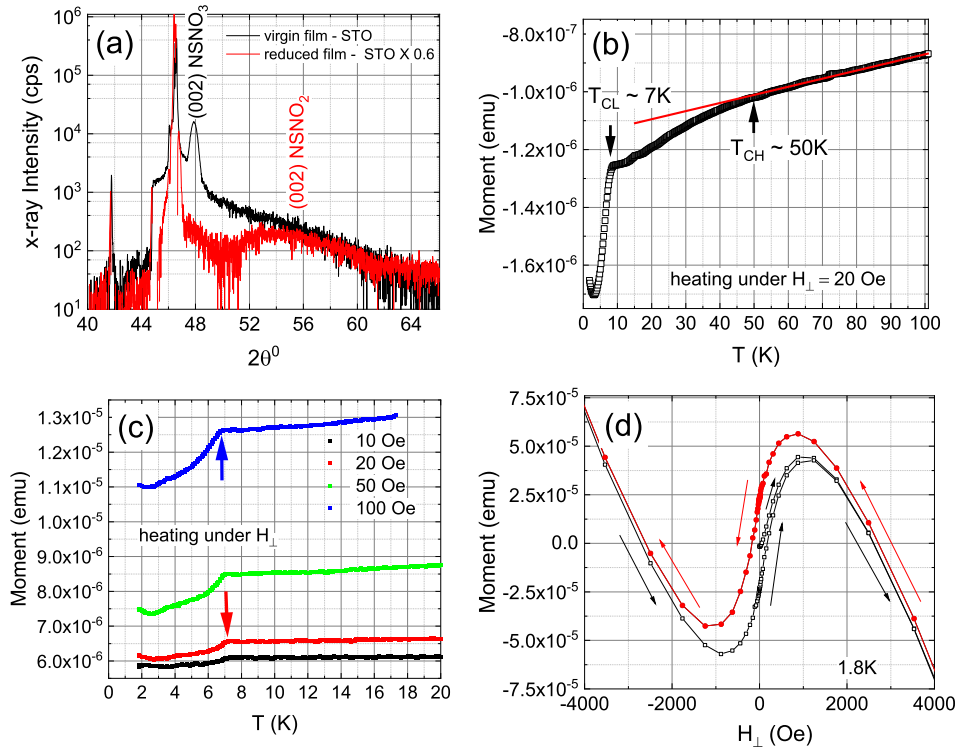


Fig. 2 XRD and magnetization results of the NSNO1red1h film (annealed in CaH_2 at 320°C for 1 h). XRD of the virgin NSNO1 and reduced NSNO1red1h films are shown in (a), where after annealing the perovskite peak of NSNO1 disappeared and the broad (002) peak of the infinite-layer $Nd_{0.8}Sr_{0.2}NiO_2$ phase appears. (b) and (c) show magnetic moments versus temperature of NSNO1red1h where two superconducting transitions are observed at about 7 and 50 K in (b), while in (c) scaling of the moment magnitude with field is demonstrated. (d) depicts a magnetic hysteresis loop of this film after ZFC, where the field was cycled to ± 5000 Oe and back to 0 Oe. The same response as in (d) is obtained also on a bare STO wafer (see Fig. 2 in section S2 of the supplemental).

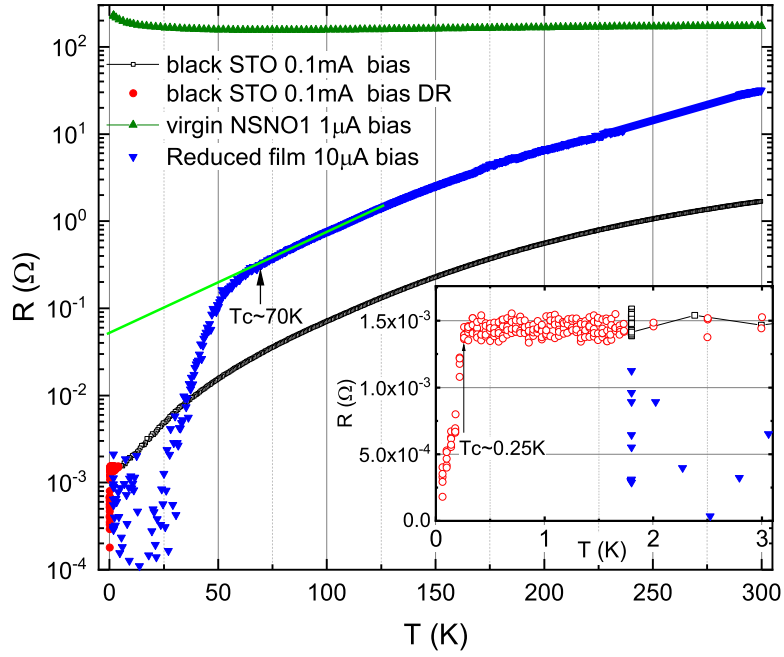


Fig. 3 Resistance versus temperature of the virgin NSNO1 film and the reduced NSNO1red1h film, together with the R vs T of a bare black STO wafer (reduced in CaH_2 at $320^{\circ}C$ for 6 h). In the inset, a zoom-in on the R vs T data of the main panel below 3 K is shown, where the red circles represent measurements obtained in a dilution refrigerator (DR). The transition to superconductivity at ~ 0.25 K is due to the highly reduced, optimally doped, black STO wafer.

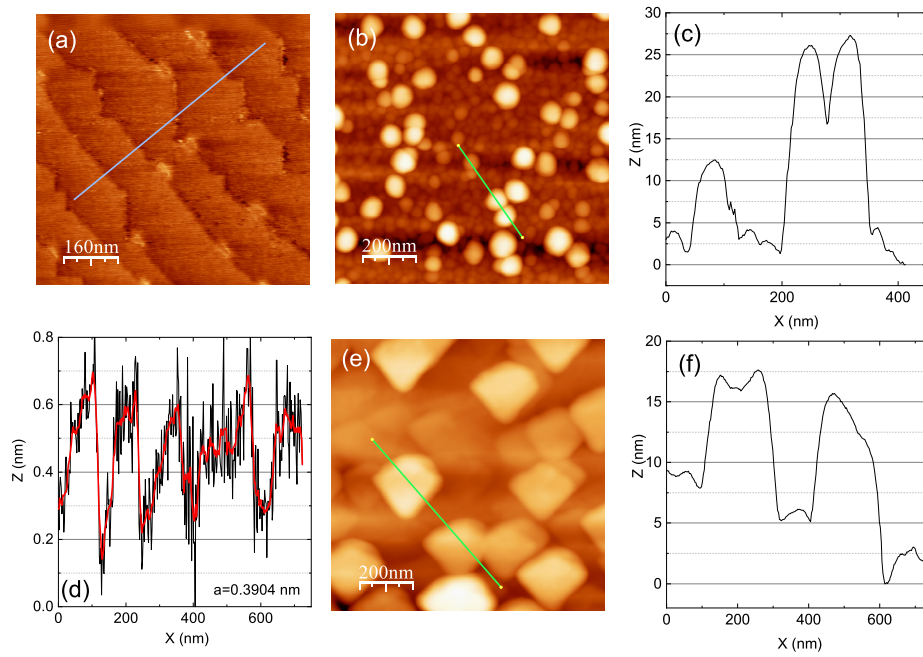


Fig. 4 An AFM image of the BHF etched and annealed STO substrate is depicted in (a), with a line-profile plotted in (d) across the terraces and along the line shown in (a). AFM images of the virgin NSNO₂ film deposited on it, and of the annealed NSNO₂red6h film (reduced in CaH_2 at 320⁰C for 6 h) are shown in (b) and (e), respectively. The typical line-profiles in (c) and (f) were obtained along the corresponding lines drawn in (b) and (e).

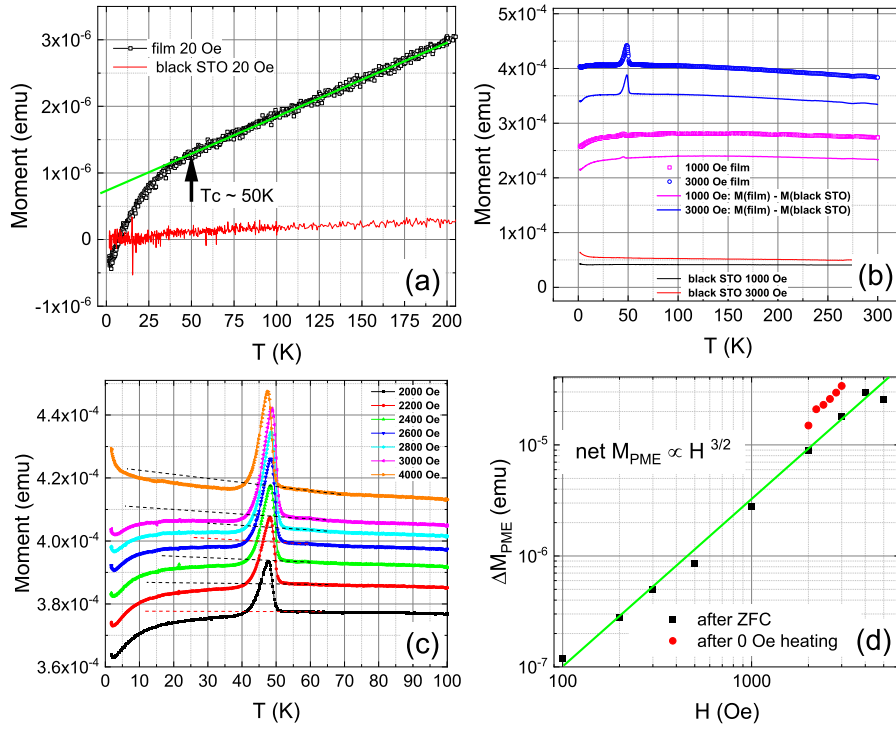


Fig. 5 (a) shows the Meissner moment versus temperature of the NSNO2red6h film and of a bare black STO wafer under the same reduction conditions. The later represents the small background contribution of the substrate to the moment of the film. The moments of this film and its bare substrate are depicted in (b) under 1000 and 3000 Oe, together with the net moments of the film after subtraction of the substrate contribution. (c) shows consecutive moment measurement results (red dots) versus temperature where the paramagnetic Meissner effect (PME) peak is robust. In (d) we plot the net PME peak magnitude versus field, where the line represent a power law behavior with exponent of $3/2$.

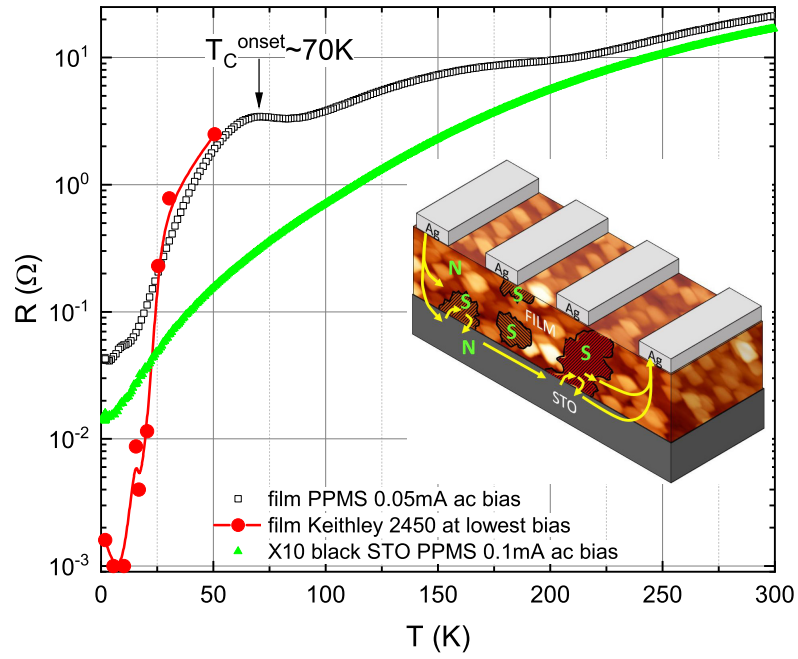


Fig. 6 Resistance versus temperature of the reduced NSNO2red6h film (black squares), together with the R vs T of a bare black STO wafer times 10 (green triangles), both measured using the PPMS system and its software. The red dots represent resistance values measured from the low bias IVCs by a Keithley 2450 source-meter, by taking into account only the minimal resistance parts of the IVCs and avoiding the resistance parts due to the diode effect (below about 20 K). The inset shows a schematic drawing of the sample, bias current flow directions and the contacts geometry, where the shaded areas represent the superconducting islands.

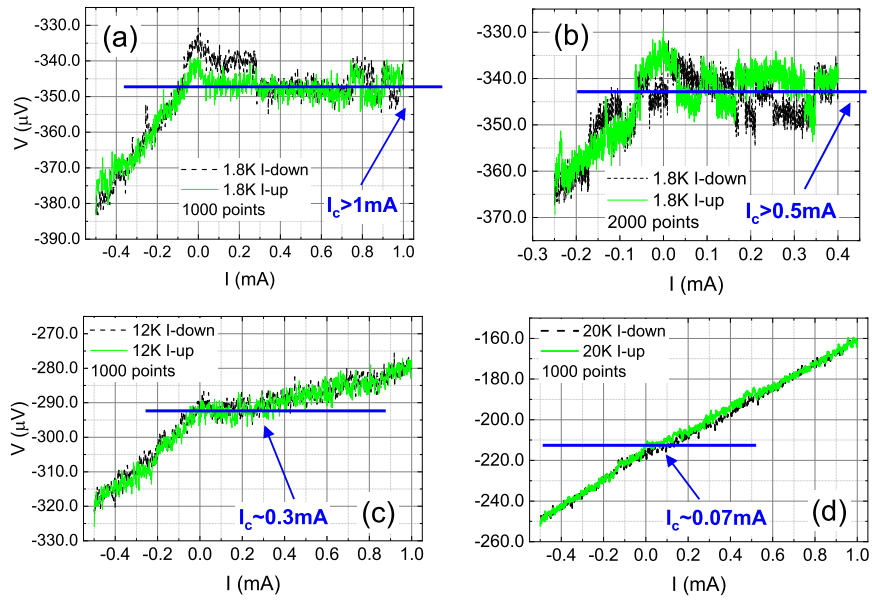


Fig. 7 Voltage versus current curves of NSNO2red6h with one week aged Ag contacts as appeared on the monitor of the Keithley 2450. No averaging was used in these measurements. (a) and (b) were taken at 1.8 K, (c) at 12 K and (d) at 20 K. Up-current scans are plotted in green, while down-current scans are plotted in black. Running voltage noise level at 1.8 K is about $5 \mu\text{V}$ and telegraph noise jumps are of about $7 \mu\text{V}$.

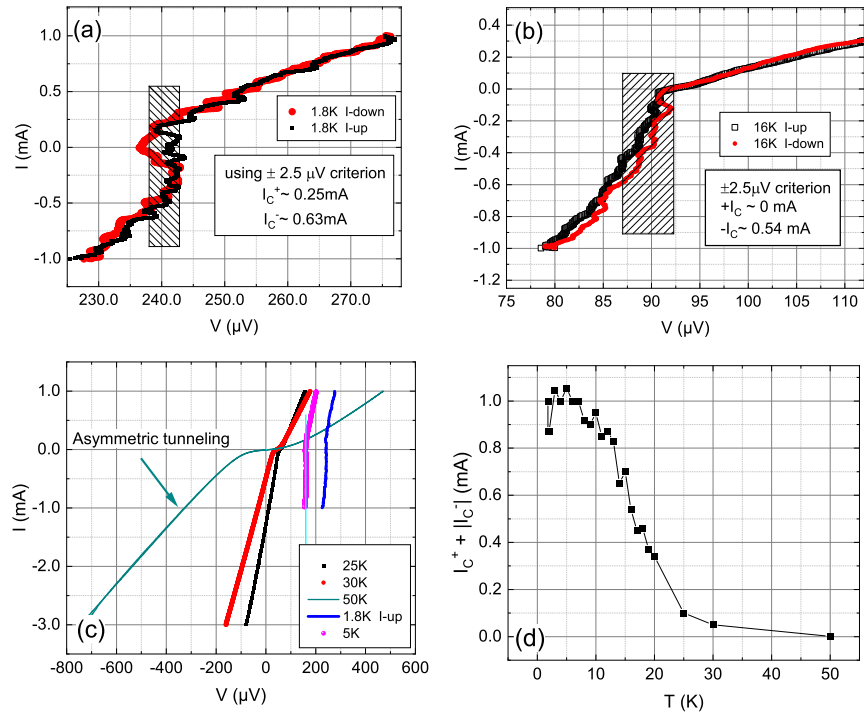


Fig. 8 Current versus voltage curves (IVCs) of the NSNO2red6h film are depicted in (a)-(c) at different temperatures, showing the asymmetric diode effect. Note the reversed polarity at low bias of these curves (more resistive at positive bias) as compared to that of Fig. 7 (more resistive at negative bias). The width of the shaded boxes in (a) and (b) represent the $\pm 2.5 \mu\text{V}$ criterion we used to determine the critical currents which are plotted in (d) versus temperature. Note that the S-shaped band near zero bias of the red curve in (a) is due to averaging over a telegraph-noise jump which isn't included in our voltage criterion (see text). (c) shows that at 50 K there is no I_c and the IVC is still asymmetric and clearly tunneling-like. It also shows the decrease with temperature of the small voltage shift from zero at zero bias.

7 Methods

We start with nickelate films grown on (100) $SrTiO_3$ (STO) substrates by pulsed laser deposition (PLD) from a ceramic target of $Nd_{0.8}Sr_{0.2}NiO_3$, resulting in the 113 perovskite phase as seen by XRD, similar to what other groups have done. This was followed by an Oxygen reduction step in CaH_2 at $320^{\circ}C$, not in a closed cell like other groups have done, but under pumping to pressures below 10^{-6} Torr, while the sample and CaH_2 powder were held in an aluminum packet with a small aperture in it at pressure of about 10^{-5} Torr (like in differential pumping). This led to an effective reduction not only of the films but also of the STO substrate, which became black and highly conductive. Separate reduced samples of bare STO wafers (without the nickelate films) were also prepared and measured, in order to serve as reference or background to the measurements of the films themselves.

Structural properties of our films were determined by standard $\theta - 2\theta$ x-ray diffraction (XRD) measurements, and the films' morphology by atomic force microscopy (AFM) images. Transport measurements of our films were carried out using a PPMS Dynacool system of Quantum Design. When high sensitivity was needed, the PPMS electronics was replaced by an external Keithley 2450 source, while still using the Dynacool's cryogenics. The contacts for the 4-probe measurements were made by a wire bonder with Al wires, and these were also overlaid by freshly applied silver paste bands for increasing the contacts area and thereby reducing their resistance by two orders of magnitude. Magnetic measurements were carried out using a Quantum Design MPMS3 SQUID magnetometer. In these measurements, the samples were placed in a straw of 5 mm diameter in a way that the applied magnetic field was perpendicular to the film's surface.

Overall, 12 nickelate films were prepared and characterized in this study using PLD with the fourth-harmonic of the Nd-YAG laser. These films were generally cut into four quarters, for reduction in CaH_2 under different annealing conditions such as temperatures, pressure and time duration. In the present study we report only on the last four films that were reduced in CaH_2 at $320^{\circ}C$ and under pumping at local pressure (in the Al packet) of about 10^{-5} Torr.

Supplementary information. A supplemental file is included with this manuscript. It presents magnetization data on bare STO substrates, measured in the same manner as the film data presented here. It also includes data from films of 10 nm and 20 nm thicknesses demonstrating superconductivity, along with comparisons to 30 nm and 35 nm films. Lastly, the file contains XRD plots of 30 nm and 35 nm thick films.

Acknowledgements. We are grateful to A. Kanigel for useful discussions.

Declarations

- There are no conflict of interest/competing interests in this article.
- Authors contribution: Anna Eyal performed the transport and magnetic measurements. Gad Koren prepared the samples and carried out the XRD and AFM characterizations. Both analyzed the data and wrote the article.

References

- Ando F, Miyasaka Y, Li T, et al (2022) Observation of superconducting diode effect. *Nature* 584:373–376
- Braunisch W, Knauf N, Bauer G, et al (1993) Paramagnetic meissner effect in high-temperature superconductors. *Phys Rev B* 48:4030–4042
- Chen X, Zhang J, Thind A, et al (2024) Polymorphism in the ruddlesden–popper nickelate $La_3Ni_2O_7$: Discovery of a hidden phase with distinctive layer stacking. *J Am Chem Soc* 146:3640–3645
- Chow SLE, Luo Z, Ariando A (2024) High-temperature superconducting oxide without copper at ambient pressure. arXiv URL <https://arxiv.org/abs/2410.00144>
- Gu Q, Li Y, Wan S, et al (2020) Two superconducting components with different symmetries in $Nd_{0.8}Sr_{0.2}NiO_2$ films. *Nat Commun* 11:6027
- He JJ, Tanaka Y, Nagaosa N (2022) A phenomenological theory of superconductor diodes. *New J Phys* 24:053014–1–9
- Ilić S, Bergeret FS (2022) Theory of the supercurrent diode effect in rashba superconductors with arbitrary disorder. *Phys Rev Lett* 128:177001–6
- Ko EK, Yu Y, Liu Y, et al (2024) Signatures of ambient pressure superconductivity in thin film $La_3Ni_2O_7$. *Nature* URL <https://www.nature.com/articles/s41586-024-08525-3>
- Koblichka MR, Pust L, Chang CS, et al (2023) The paramagnetic meissner effect (pme) in metallic superconductors. *Metals* 13:1140

- Koren G, Gupta A, Baseman RJ, et al (1989) Laser wavelength dependent properties of $YBa_2Cu_3O_{7-\delta}$ thin films deposited by laser ablation. Appl Phys Lett 55:2450–2452
- Koren G, Eyal A, Iomin L, et al (2021) Observation of josephson-like tunneling junction characteristics and positive magnetoresistance in oxygen deficient nickelate films of $Nd_{0.8}Sr_{0.2}NiO_{3-\delta}$. Materials 14:7689–1–13
- Lee K, Wang BY, Osada M, et al (2023) Linear-in-temperature resistivity for optimally superconducting $(Nd, Sr)NiO_2$. Nature 619:288–292
- Lee Y, Wei X, Yu Y, et al (2024) Millimeter-scale freestanding superconducting infinite-layer nickelate membranes. arXiv URL <https://arxiv.org/abs/2402.05104>
- Li D, Lee K, Wang BY, et al (2019) Superconductivity in an infinite-layer nickelate. Nature 572:624–627
- Li D, Wang BY, Lee K, et al (2020a) Superconducting dome in $Nd_{1-x}Sr_xNiO_2$ infinite layer films. Phys Rev Lett 125:027001
- Li Q, He C, Si J, et al (2020b) Absence of superconductivity in bulk $Nd_{0.8}Sr_{0.2}NiO_2$. Commun Mat 16:1–8
- Lin X, Bridoux G, Gourgout A, et al (2014) Critical doping for the onset of a two-band superconducting ground state in $SrTiO_{3-\delta}$. Phys Rev Lett 112:207002–1–5
- Linder J, Balatsky AV (2019) Odd-frequency superconductivity. Rev Mod Phys 91:045005–1–56
- Liu Y, Ko EK, Tarn Y, et al (2025) Superconductivity and normal-state transport in compressively strained $La_2PrNi_2O_7$ thin films. arXiv URL <https://arxiv.org/abs/2501.08022>

- Mori M, Koshibae W, Maekawa S (2025) Towards optimization of the josephson diode effect. arXiv URL <https://arxiv.org/abs/2501.05671>
- Moshchalkov VV, Qiu XG, Bruyndoncx V (1997) Paramagnetic meissner effect from the self-consistent solution of the ginzburg-landau equations. *Phys Rev B* 55:11793–11801
- Norman MR (2020) Entering the nickel age of superconductivity. *Physics* 13:85
- Osada M, Wang B, Goodge B, et al (2020) A superconducting praseodymium nickelate with infinite layer structure. *Nano Lett* 20:5735
- Puphal P, Wu YM, Fürsich K, et al (2021) Topotactic transformation of single crystals: From perovskite to infinite-layer nickelates. *Sci Adv* 7:eabl8091
- Qi S, Ge J, Ji C, et al (2025) High-temperature field-free superconducting diode effect in high- T_c cuprates. *Nature Comm* 16:531
- Riedling S, Bräuchle G, Lucht R, et al (1994) Observation of the wohlleben effect in $\text{YBa}_2\text{Cu}_3\text{O}_{7-\delta}$ single crystals. *Phys Rev B* 49:13283
- Sun H, Huo M, Hu X, et al (2023) Signatures of superconductivity near 80 k in a nickelate under high pressure. *Nature* 621:493–498
- Yamada H, Miller GR (1973) Point defects in reduced strontium titanate. *Jour Solid State Chem* 6:169–177
- Yuan NFQ, Fu L (2022) Supercurrent diode effect and finite-momentum. *PNAS* 119:e2119548119
- Zeng S, Tang C, Yin X, et al (2020) Phase diagram and superconducting dome of infinite-layer $\text{Nd}_{0.8}\text{Sr}_{0.2}\text{NiO}_2$ thin films. *Phys Rev Lett* 125:147003

Zhang Y, Pei C, Guo N, et al (2025) Damage of bilayer structure in $La_3Ni_2O_{7-\delta}$ induced by high p_{O_2} annealing. arXiv URL <https://arxiv.org/abs/2502.01501>

Zhou G, Lv W, Wang H, et al (2024) Ambient-pressure superconductivity onset above 40 k in bilayer nickelate ultrathin films. arXiv URL <https://arxiv.org/abs/2412.16622>

Zhou X, Feng Z, Qin PX, et al (2020) Absence of superconductivity in $Nd_{0.8}Sr_{0.2}NiO_2$ thin films without chemical reduction. Rare Met 39:368–374

Supplemental

for

Experimental evidence of T_c enhancement above
50 K and diode and paramagnetic-Meissner
effects, in Nickelate films on highly reduced
 $SrTiO_3$

by:

Anna Eyal and Gad Koren

Physics Department, Technion-Israel Institute of Technology
Haifa, Israel

February 20, 2025

Abstract

In this supplemental we provide additional evidence for the T_c enhancement over 50 K found in our reduced nickelate films. This is done by presenting transport and magnetization results measured on 20 and 10 nm thick films, where T_c onset of 50-60 K is found again. The independence of this result of the films' thickness (including the 30 and 35 nm films of the main article) further supports the notion that superconductivity in these films is an interface effect. Also given here are the hysteresis loop of bare black STO indicating its ferromagnetic nature, and XRD results showing the need for better x-ray sources with higher resolution.

1 S1: XRD of the 35 and 30 nm thick films

Figure 1 (a) depicts XRD spectra of the NSNO2red6h film. Clearly, if there are any film peaks, they are within the noise level of this measurement, or hidden under the strong (n00) peaks of the STO substrate. (b) shows a smaller XRD range near the (200) peak of the STO substrate, where results of the virgin films NSNO1 and NSNO2 together with the annealed film NSNO2red6h are plotted. Both virgin films before the annealing have prominent (002) peaks of the perovskite $Nd_{0.8}Sr_{0.2}NiO_3$ phase. After 6h annealing in CaH_2 at $320^{\circ}C$ of the NSNO2 film that produced the NSNO2red6h film, the (002) film peak disappeared, and there is still no clear trace of any other film peaks besides those of the STO wafer, unless the "knee" at 48° is due to the film and isn't a side-band of the huge (200) peak of STO. We conclude that if there are any film peaks besides this knee, they are probably broad and hidden in the noise of the present XRD measurement.

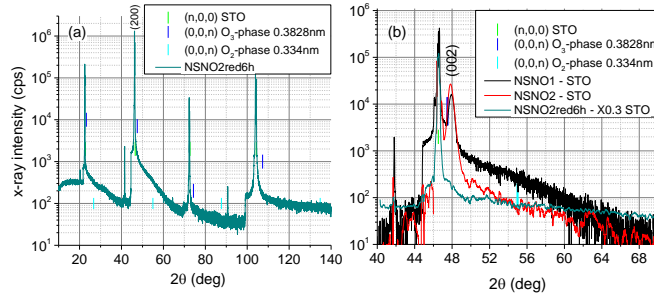


Figure 1: (a) Full range XRD of the NSNO2red6h film. (b) XRD of the NSNO1, NSNO2 and NSNO2red6h films near the (200) peak of the (100) STO wafer. The "knee" at 48° could be due to the film, or represents a side-band of the huge (200) peak of the STO wafer.

2 S2: M vs H of a bare STO wafer

Figure 2 shows the magnetic moment at 1.8 and at 100 K versus perpendicular magnetic field of a virgin (100) STO wafer without a nickelate film and without annealing in CaH_2 . The field was cycled from 0 Oe to ± 5000 Oe and back to 0 Oe. The data sets were taken after ZFC. The coercive field of ~ 750 Oe at 1.8 K was reduced to ~ 550 Oe at 100 K. Clearly, the bare STO substrate is ferromagnetic, and the response at 1.8 K here is similar to that of the reduced NSNO1red1h sample of Fig. 2 (d) of the main article.

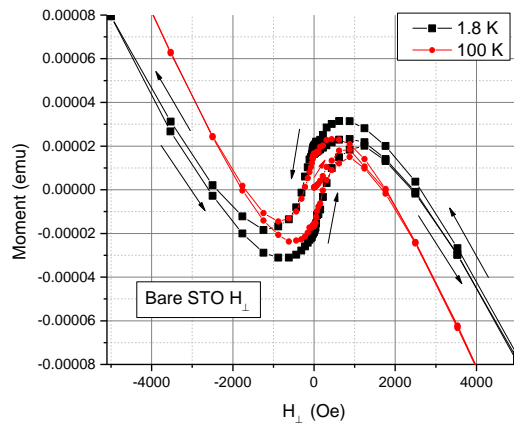


Figure 2: Moment versus perpendicular magnetic field of a bare STO wafer at 1.8 and 100 K. The arrows show the magnetic field cycling sequence starting and ending at 0 Oe.

3 S3: $T_c \sim 50$ K of a 20 nm thick film

In addition to the 30 and 35 nm thick films described in the main article, we also prepared films of 10 and 20 nm thickness. These films were not as extensively characterized, but here in Fig. 3 we present magnetization moment measurements versus temperature of a 20 nm thick film that was reduced for 1.5 h in CaH_2 at 320°C . One can see that the high-temperature transition at ~ 50 K is well reproduced, supporting the notion of a robust superconducting transition at 50 K. The inset to this figure shows the net magnitude of the moments between 20 and 50 K of this film versus reduction time, as well as those of the main article. One can see that these net moments are almost linear in the duration of their reduction time and almost independent of the films' thicknesses in this range. This result indicates that it is most likely that the moments originate at the interface of these films and substrates, regardless of their thickness down to 20 nm. Figure 4 of the next S4 section shows that this is true also down to 10 nm.

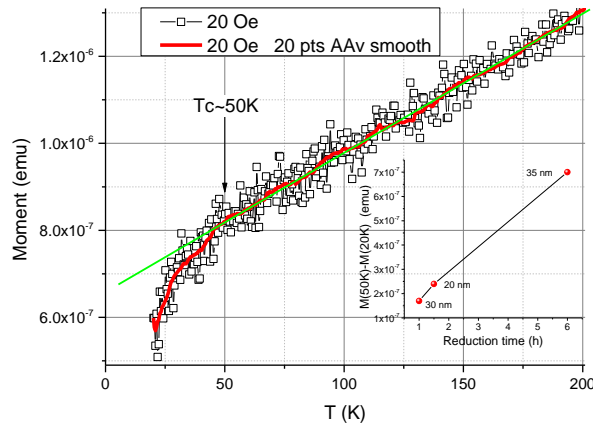


Figure 3: Moment versus temperature of a 20 nm thick NSNO3red1.5h film measured under 20 Oe field. This film was reduced for 1.5 h in CaH_2 at 320°C under pumping at $\sim 10^{-5}$ Torr. The measurement was carried out under heating from 20 K after field cycling to ± 5000 Oe at 1.8 K. The inset shows the net moments between 20 and 50 K of three films (NSNO1red1h, NSNO3red1.5h and NSNO2red6h of thicknesses 30, 20 and 35 nm, respectively) versus their reduction time.

4 S4: R vs T of a 10 nm thick film

Though we do not have magnetic moment results on our 10 nm thick film (NSNO4red2h, reduced in CaH_2 at $320^{\circ}C$ for 2 h), we do have transport result on it. Figure 4 depicts two resistance versus temperature results under low and high bias currents as measured by the PPMS system. We measured many IVCs using this system on this film and found very nonlinear behaviors at low temperatures. Nevertheless, at very low bias the IVCs were almost linear, but quite noisy. Therefore, the R vs T here at low T and $1 \mu A$ bias, which we ignored at the beginning, is actually the more reliable result. If we consider the 1 mA bias result, down to about 50 K, as a background mostly due to the black STO substrate, then any deviation from it marks the onset of a possible superconducting transition. One can see that such a deviation of the $1 \mu A$ biased curve occurs at about 60 K. Without the data of the main article, we would have continue to ignore the results of Fig. 4 here, but this data actually further support the existence of a superconducting transition above 50 K (60 K here), as was clearly demonstrated in the main article.

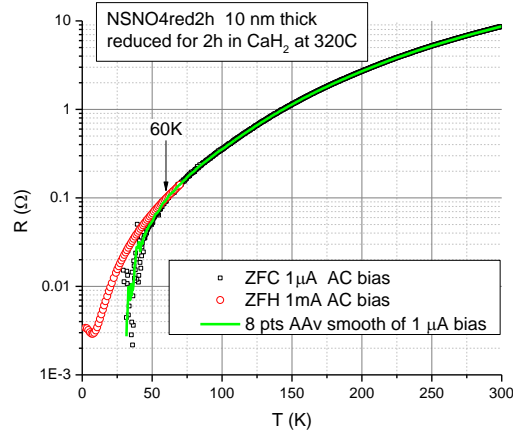


Figure 4: R versus T of NSNO4red2h, a 10 nm thick film, as measured by the PPMS system at $1 \mu A$ and 1 mA bias. At low temperatures, the IVCs are linear only very close to zero bias due to the diode effect (see Figs. 7 and 8 of the main article). Therefore, the 1 mA bias result at low temperatures is misleading and shows finite resistance below 30 K (see a similar behavior when using the PPMS system in Fig. 6 of the main article). Therefore, the noisy data under $1 \mu A$ bias at low temperatures is more reliable. It shows a transition onset (deviation from the 1 mA bias result) already at about 60 K.